Structure and Surface and Catalytic Properties of Mg-Al Basic Oxides

J. I. Di Cosimo,* V. K. Díez,* M. Xu,† E. Iglesia,† and C. R. Apesteguía*,1

*Instituto de Investigaciones en Catálisis y Petroquímica (INCAPE), Santiago del Estero 2654, (3000) Santa Fe, Argentina;
and †Department of Chemical Engineering, University of California at Berkeley, Berkeley, California 94720

Mg-Al mixed oxides with Mg/Al molar ratios of 0.5–9.0 were obtained by thermal decomposition of precipitated hydrotalcite precursors. The effect of composition on structure and surface and catalytic properties was studied by combining several characterization methods with ethanol conversion reactions. The nature, density, and strength of surface basic sites depended on the Al content. On pure MgO, strong basic sites consisted predominantly of O^{2-} anions. Calcined hydrotalcites contained surface sites of low (OH^- groups), medium (Mg-O pairs), and strong (O^{2-} anions) basicity. The relative abundance of low and medium strength basic sites increased with the Al content. The addition of small amounts of Al to MgO diminished drastically the density of surface basic sites because of a significant Al surface enrichment. Formation of surface amorphous AlO_y structures in samples with low Al content (Mg/Al > 5) partially covered the Mg-O pairs and decreased the concentration of surface O^{2-} anions. At higher Al contents (5 > Mg/Al > 1), the basic site density increased because the Al^{3+} cations within the MgO lattice created a defect in order to compensate the positive charge generated, and the adjacent oxygen anions became coordinatively unsaturated. In samples with Mg/Al < 1, segregation of bulk $MgAl_2O_4$ spinels occurred and caused the basic site density to diminish. The catalyst activity and selectivity of Mg-Al mixed oxides in ethanol conversion reactions depended on composition. The dehydrogenation of ethanol to acetaldehyde and the aldol condensation to *n*-butanol both involved the initial surface ethoxide formation on a Lewis acid–strong base pair. Pure MgO exhibited poor activity because the predominant presence of isolated O^{2-} basic centers hindered formation of the ethoxide intermediate by ethanol dissociative adsorption. The incorporation of small amounts of Al^{3+} cations to MgO drastically increased the acetaldehyde formation rate because of the generation of new surface Lewis acid–strong base pair sites. Acetaldehyde condensation toward *n*-butanol is a bimolecular reaction between adjacent adsorbed acetaldehyde species that requires not only acid–strong base pair sites but also a high density of basic sites; these pathways were favored on Mg-Al samples with higher Al content (5 > Mg/Al > 1). The dehydration of ethanol to ethylene, and the coupling and dehydration to diethyl ether increased with Al content, probably reflecting the density increase of both Al^{3+}-O^{2-} pairs and low- and medium-strength basic sites. Pure Al_2O_3 displayed the highest dehydration activity. © 1998 Academic Press

1 Corresponding author. E-mail: capesteg@fiqus.unl.edu.ar.

INTRODUCTION

Layered double hydroxides are anionic clays in which divalent cations within brucite-like layers are replaced by trivalent cations. The resulting positive charge is compensated by hydrated anions located in the interlayer space between two brucite sheets. The general formula for these materials is $[M_{1-x}^{II} M_x^{III} (OH)_2]^{x+} (A_{x/n})^{n-} \cdot$ m H_2O, where M^{II} is a divalent cation, such as Mg^{2+}, Mn^{2+}, Fe^{2+}, Co^{2+}, Cu^{2+}, Ni^{2+}, Zn^{2+}, or Ca^{2+}; M^{III} is a trivalent cation, such as Al^{3+}, Cr^{3+}, Mn^{3+}, Fe^{3+}, Co^{3+}, or La^{3+}, and A^{n-} is the anion (1). Hydrotalcites and hydrotalcite-like compounds belong to this class of materials.

Hydrotalcite-derived mixed oxides are used as antacids, ion exchangers, and absorbers, and catalysts and catalyst supports, because of their high surface area, phase purity, basic surface properties, and structural stability (2). Hydrotalcite-derived oxides catalyze higher alcohol synthesis from CO/H_2 (3), oxidation of mercaptans (4), water gas shift reactions (5). Also, Mg-Al mixed oxides prepared by oxidative decomposition of hydrotalcite precursors have been used in base-catalyzed aldol condensation (6, 7), alkylations (8), Knoevenagel condensations (9), double-bond isomerization (7), and alcohol dehydrogenation and coupling (10).

The structure and surface properties of Mg-Al hydrotalcites and of the resulting mixed oxides depend strongly on chemical composition and synthesis procedures (2). In catalysis, surface area, intimate contact between two or more oxide components, and the size of the resulting metal oxide clusters strongly influence the rate and selectivity of chemical reactions. Shaper *et al.* (11) studied the activity of calcined Mg-Al hydrotalcites with low Al content (Mg : Al atomic ratios between 5 and 15) in the double-bond isomerization of 1-pentene. They found that the sample activity depends strongly on chemical composition and calcination temperature. Mg-Al hydrotalcites calcined at 773 K displayed strong basicity and they were more active than pure MgO. Velu and Swamy (8) studied the alkylation of phenol with methanol on Mg-Al calcined hydrotalcites with Mg : Al ratios from 3 to 10. The Mg-Al 4 : 1 ex-hydrotalcite was the

most active sample, exhibiting also the highest selectivity for 2,6-xylenol formation. The authors concluded that the participation of both acidic and basic sites is required for alkylation reactions and that surface acid-base properties are determined by the Al content. The influence of chemical composition of Mg-Al calcined hydrotalcites on the dehydrogenation of isopropanol was investigated by Corma *et al.* (12). They prepared samples with different Mg/Al ratios and found a maximum in dehydrogenation activity for samples with a Mg/Al ratio of 3. For reactions requiring stronger basicity, maximum rates were observed at higher Mg/Al ratios. This work showed that on calcined Mg/Al hydrotalcites the surface acid–base properties and, as a consequence, the catalytic activity and selectivity depend on chemical composition. Intermediate Mg/Al compositions may show unique catalytic properties, which depend on the reaction requirements for the density and strength of basic sites.

In this study, we prepared calcined Mg-Al hydrotalcites with Mg/Al molar ratios of 0.5–9.0. The effect of composition on structure and surface and catalytic properties was studied by combining several characterization methods with chemical reactions using probe molecules. The crystal structure and crystallite size were determined by X-ray diffraction (XRD). Surface composition was measured by X-ray photoelectron spectroscopy (XPS). The density and reactivity of basic sites were determined using $^{13}CO_2/^{12}CO_2$ isotopic switch methods and catalytic reactions of ethanol. The density, binding energy, and structure of CO_2 chemisorbed on basic sites were examined by temperature-programmed desorption and infrared spectroscopy of adsorbed CO_2.

METHODS

Synthesis Procedures

Five Mg-Al hydrotalcite precursors with different Mg/Al atomic ratios were prepared by co-precipitation of an aqueous solution of $Mg(NO_3)_2 \cdot 6 H_2O$ and $Al(NO_3)_3 \cdot 9 H_2O$ containing the desired Mg/Al ratio at a constant pH of 10. A solution with a total $[Mg + Al]$ cation concentration of 1.5 M was contacted with a basic solution of K_2CO_3 and KOH by dropwise addition of both solutions into a stirred beaker containing 350 cm^3 of distilled deionized water held at 333 K. The precipitates formed were aged in their mother liquor for 2 h at 333 K and then filtered, washed with boiling distilled water until K^+ was no longer detected in the filtrate, and dried at 348 K overnight. These hydroxycarbonate precursors (HT samples) were decomposed in N_2 at 673 K overnight in order to obtain the corresponding Mg-Al mixed oxides (CHT samples). Pure alumina and MgO were prepared following the same procedure.

Methods for the Characterization of Structure and Surface Properties

The solid structure and crystal size in HT and CHT samples were determined by powder X-ray diffraction methods using a Shimadzu XD-D1 diffractometer and Ni-filtered CuKα radiation.

The density of basic sites available for reversible adsorption-desorption of CO_2 on CHT samples were measured at 473 and 573 K by isotopic $^{13}CO_2/^{12}CO_2$ exchange methods (13). In this method, a sample is exposed to a 0.1% $^{13}CO_2$/0.1% Ar/He stream at 473 K or 573 K until $^{13}CO_2$ concentrations in the effluent reach a constant value and then the stream is rapidly replaced with one consisting of 0.1% $^{12}CO_2$/He. The number and rate of evolution of preadsorbed $^{13}CO_2$ is then measured by continuous monitoring of the effluent stream by mass spectrometry as a function of time elapsed since the isotopic switch. Ar is present in one of the streams in order to correct the exchange dynamics for gas holdup and hydrodynamic delays within the experimental apparatus.

CO_2 binding energies were determined by temperature-programmed desorption (TPD) of CO_2 preadsorbed at room temperature. Samples (50 mg) were treated in He at 723 K for 0.3 h and exposed to a 0.1% CO_2/0.1% Ar/He stream at room temperature until saturation coverages were reached. Weakly adsorbed CO_2 was removed by flushing with He at room temperature for about 0.3 h. The temperature was then increased at a linear rate of 0.5 K/s from 298 to 723 K and the rate of CO_2 evolution was monitored by mass spectrometry.

The structure of CO_2 chemisorbed on hydrotalcite-derived samples was determined by infrared spectroscopy (IR). Data were obtained using a Shimadzu FTIR-8101M spectrophotometer after CO_2 adsorption at room temperature and sequential evacuation at 298, 373, 473, 573, and 623 K. Spectra were taken at room temperature. An inverted T-shaped Pyrex cell containing the sample pellet was used. The two ends of the short arm of the T were fitted with CaF$_2$ windows. The absorbance scales were normalized to 50-mg pellets.

The surface composition of CHT samples was measured by X-ray photoelectron spectroscopy (XPS) using a Shimadzu ESCA-750 spectrometer and the integrated areas corresponding to the O 1s, Mg 2s, and Al 2s lines. XPS binding energies were calibrated by reference to the position of the C 1s signal at 284.6 eV. Bulk elemental analysis of Mg, Al, and K was carried out by atomic absorption spectroscopy (AAS). Total surface areas (Sg) were measured by N_2 physisorption at 77 K using a Quantachrome Nova-1000 sorptometer and BET analysis methods. Prior to N_2 physisorption, the hydrotalcite precursors and calcined hydrotalcites were outgassed for 1 h at 393 K and 623 K, respectively.

Ethanol Reaction Procedures

Catalytic testing was carried out at 573 K and 100 kPa in a plug-flow fixed-bed reactor. Ethanol (Merck ACS, 99.8% purity) was introduced as a 1:10 ethanol/N_2 mixture. Before catalytic tests, the samples were pretreated in nitrogen at 673 K for 1 h in order to remove water and carbon dioxide. Catalyst loadings of 200 mg, sieved at 0.35–0.42 mm, and contact times of 46 g catalyst h/mol of ethanol were used. Diffusional limitations were ruled out by varying particle sizes and contac times between 0.15–0.49 mm and 4–120 g catalyst h/mol of ethanol, respectively. The reaction products were analysed by on-line gas chromatography using a ATI Unicam 610 chromatograph equipped with flame ionization detector and a 0.2% Carbowax 1500/80-100 Carbopack C column. Data were collected every 0.5 h for 10 h. The predominant reaction products were acetaldehyde, n-butanol, diethyl ether, ethylene, and n-butyraldehyde. Traces of ethyl acetate, 2-propanol, 2-pentanone, and acetone were also detected.

RESULTS

Structural Characterization of Hydrotalcite Precursors (HT)

The nominal chemical composition, BET surface area and crystalline phases are shown in Table 1 for $Mg_{(1-x)}Al_x$ samples before hydrotalcite decomposition (HT samples). X-ray diffraction patterns show a single crystalline phase with hydrotalcite structure for values of $x = Al/(Al + Mg)$ between 0.1 and 0.67. Outside this composition range, phases containing only Mg or Al were also detected (e.g., $Al(OH)_3$ (bayerite, ASTM 20-11), $Mg(OH)_2$ (brucite, ASTM 7-239)). Diffraction patterns are consistent with the proposed hydrotalcite structure, consisting of layered double hydroxides with brucite-like layers and $[Mg_{1-x}Al_x(OH)_2]^{x+}(CO_3)^{2-}_{x/2} \cdot mH_2O$ composition. The stoichiometric hydrotalcite structure, $Mg_6Al_2(OH)_{16}CO_3 \cdot 4H_2O$ (ASTM 14-191) is reached when x is 0.25. The unit cell constants (a and c) for hydrotalcite struc-
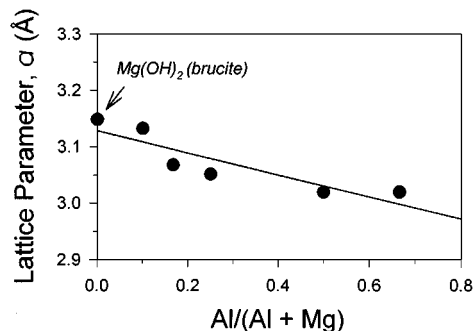

FIG. 1. HT samples: unit cell parameter, a, as a function of the chemical composition. Brucite included as a reference.

tures with hexagonal 3R symmetry were calculated on all HT samples from X-ray diffraction patterns and values of a are shown in Fig. 1 as a function of the $Al/(Al + Mg)$ atomic ratio. The value of a decreases linearly with increasing Al content from its initial value for brucite structures not containing Al (3.148 Å). Sharp X-ray diffraction lines were detected in sample HT3, which has the composition of the stoichiometric hydrotalcite ($x = 0.25$). All other samples show broader XRD lines, corresponding to smaller crystallites or less ordered structures, as shown by the crystallite diameter values calculated from XRD line breadths and reported in Table 1 for HT samples. The BET surface areas of HT samples were between 65 and 85 m^2/g and showed no systematic dependence on composition.

Structural Characterization of CHT Mixed Oxide Samples

The chemical composition, BET surface area, and crystalline phases for $Mg_{(1-x)}Al_xO$ samples formed by decomposition of hydrotalcite precursors (CHT) are shown in Table 2. Data on pure MgO and Al_2O_3 are also included in Table 2. Elemental analysis of CHT samples gave $Al/(Al + Mg)$ atomic ratios very similar to those present in the precursor solution, consistent with complete precipitation of Mg and Al salts during synthesis. The potassium content in all CHT samples was below 0.1 wt%, which confirms that K^+ ions were effectively removed by filtration and washing of the precipitated precursors.

Thermal decomposition of hydrotalcite precursors led to the formation of high surface area Mg-Al oxides. Surface areas were significantly higher than in HT samples (Tables 1 and 2); it appears that the removal of CO_2 during decomposition leads to the formation of significant porosity. This is consistent with the increase in surface area as the Al (and the CO_3^{2-}) content on HT samples increases. All CHT samples showed diffraction patterns consistent with the presence of a crystalline MgO periclase phase (ASTM 4-0829). Sample CHT5 also has an additional $MgAl_2O_4$ spinel phase (ASTM 21-1152). Crystalline AlO_y phases were not detected in any of the CHT samples. The

TABLE 1

HT Samples: Chemical Composition, BET Surface Areas, and XRD Characterization

Sample	Nominal molar composition $x = Al/(Al + Mg)$	Sg (m^2/g)	XRD analysis Phase	XRD analysis Crystallite size (Å)
HT1	0.10	71	Hydrotalcite + brucite	54
HT2	0.17	69	Hydrotalcite	101
HT3	0.25	76	Hydrotalcite	106
HT4	0.50	66	Hydrotalcite	99
HT5	0.67	85	Hydrotalcite + bayerite	75

TABLE 2

CHT Samples: Chemical Composition, BET Surface Areas and XRD Characterization

Sample	Elemental analysis[a]				Sg (m^2/g)	XRD analysis		
	Al/(Al + Mg) (molar)	Mg (wt%)	Al (wt%)	K (wt%)		Phase	Crystallite size (Å)	Lattice parameter (Å)
MgO	0.00	—	—	0.003	125	MgO	75	4.213
CHT1	0.11	45.3	6.2	0.008	114	MgO	124	4.208
CHT2	0.18	39.7	9.7	0.020	184	MgO	91	4.211
CHT3	0.24	34.4	12.1	0.020	238	MgO	28	4.216
CHT4	0.47	22.2	21.5	0.080	231	MgO	21	4.209
CHT5	0.65	15.0	31.1	0.085	298	$MgO + MgAl_2O_4$	<20	-
Al_2O_3	1.00	-	-	0.060	388	Amorphous	-	-

[a] By AAS.

crystallinity of CHT samples and the apparent crystallite size decreased with increasing Al content (Table 2). Higher surface areas and smaller crystallites are strongly favored by high Al contents in CHT samples.

Surface Properties of CHT $Mg_{(1−x)}Al_xO$ Samples

The surface composition of MgO, Al_2O_3, and CHT $Mg_{(1−x)}Al_xO$ samples was measured by X-ray photoelectron spectroscopy. The surface atomic fraction of oxygen, aluminum, and magnesium are designated as O_s, Al_s, and Mg_s, respectively. The corresponding bulk molar fractions, O_b, Al_b, and Mg_b, were obtained from bulk elemental analysis (Table 2). XPS results are shown in Table 3. The O 1s binding energy (Table 3, column 2) changes with chemical composition, suggesting that the chemical form of the surface oxygen species depends on chemical composition. The measured O 1s binding energy increases as the Al content increases, from values typical of surface $O^{2−}$ (14, 15) on pure MgO (529.5 eV), to that characteristic of surface hydroxide (16) on pure Al_2O_3 (531.8 eV). The amount of

surface oxygen also depends on chemical composition. In Fig. 2, the O_s/O_b ratio is shown as a function of Al content. Pure MgO exhibits the highest surface oxygen concentration, with a value of $O_s/O_b = 0.92$. In CHT samples, the O_s/O_b ratio depends on chemical composition, with a minimum value reached at a low Al content and then a broad maximum appearing at higher Al contents.

As expected, Al_s and Mg_s values follow qualitative trends that parallel the bulk sample composition. As x increases, Al_s increased and Mg_s decreased (Table 3). As the Al content in CHT samples increased, however, Al_s/Al_b ratios decreased and Mg_s/Mg_b ratios increased. Samples CHT1 and CHT2 showed segregation of Al to the surface and the Al_s/Al_b ratio (2.30–2.68) is much higher than in pure Al_2O_3 (1.13) (Table 3). In CHT samples with low Al content ($x < 0.18$), Mg_s/O_s ratios were very similar to those in MgO, but these ratios decreased as the Al content increased. Al_s/O_s ratios were between 0.3 and 0.6 in all samples; these values are much lower than in pure Al_2O_3 (0.82).

$^{13}CO_2/^{12}CO_2$ isotopic exchange measurements at 473 K and 573 K give the density of basic sites available for

TABLE 3

Characterization of CHT Samples: XPS and TPD Results

Sample	Surface analysis by XPS					TPD of adsorbed CO_2			
	O 1s B. E.[a] (eV)	Mg_s/Mg_b	Al_s/Al_b	Al_s/O_s	Mg_s/O_s	l.t.p.	m.t.p.	h.t.p.	Total evolved CO_2 (μmol/m²)
MgO	529.5	1.08	—	—	1.20	4.9	35.9	59.3	1.63
CHT1	530.5	1.35	2.68	0.31	1.26	20.0	37.3	42.7	1.17
CHT2	530.1	1.42	2.30	0.41	1.16	16.7	37.6	45.7	0.46
CHT3	530.6	1.47	1.74	0.33	0.90	14.6	39.6	45.8	0.59
CHT4	530.8	1.55	1.38	0.40	0.50	21.9	44.5	33.6	0.83
CHT5	531.2	2.50	1.20	0.63	0.70	23.2	44.2	32.6	0.73
Al_2O_3	531.8	-	1.13	0.82	-	48.6	51.4	0.0	0.34

[a] Binding energy.
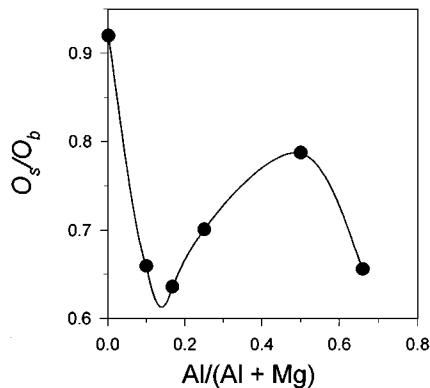[b] L.t.p: low-temperature peak; m.t.p.: middle-temperature peak; h.t.p.: high-temperature peak.

FIG. 2. Surface/bulk oxygen ratio in MgO and CHT samples as a function of the chemical composition.

FIG. 4. Isotopic exchange experiments at 473 K and 573 K; density of basic sites on MgO and CHT samples as a function of the chemical composition.

reversible CO_2 adsorption at these temperatures. Figure 3 shows isotopic exchange rates as a function of time on pure MgO and CHT samples at 573 K and the corresponding relaxation curve for the inert Ar tracer. The areas under the relaxation curves in Fig. 3, after corrections for gas holdup, physical hydrodynamic delays, and CO_2 mass spectrometric response factors, represent the exchange capacity, i.e. the density of basic sites that reversibly chemisorb CO_2 at 573 K. Basic site densities measured on pure MgO and CHT samples at 473 K and 573 K are shown in Fig. 4 as a function of chemical composition. Basic site densities measured at 473 K are slightly higher than those obtained at 573 K, because weaker binding sites are unable to maintain measurable CO_2 coverages at the higher temperature. Basic site densities were higher on MgO than on CHT samples. At 573 K, the chemisorption capacity on MgO was 0.40 μmol/m^2, while it was only 0.17 μmol/m^2 on sample

CHT1, which contains 6.2 wt% Al. Increasing the Al content led to a second maximum in site density at 0.33 μmol/m^2 for sample CHT4 ($x = 0.47$).

A qualitative measure of the basic site strength and the structure of chemisorbed CO_2 were obtained by TPD and infrared measurements of preadsorbed CO_2. The rate of CO_2 evolution as a function of sample temperature is shown in Fig. 5 for MgO, Al_2O_3, and CHT samples. The total
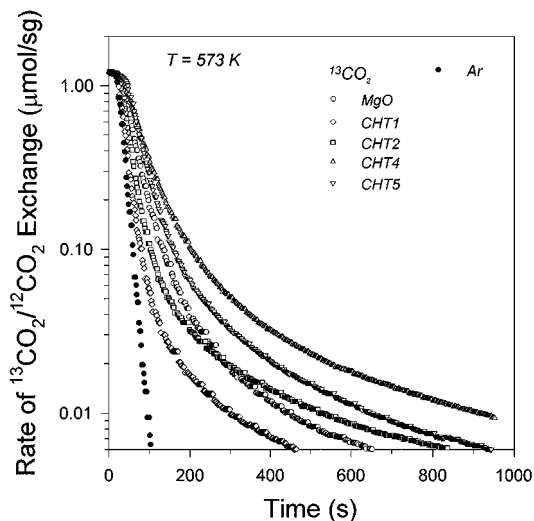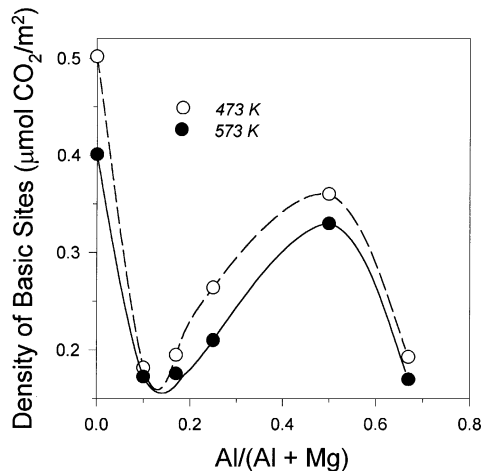

FIG. 3. Isotopic exchange experiments at 573 K; relaxation of $^{13}CO_2$ as a function of time on MgO and CHT samples. Relaxation of Ar included as a reference.
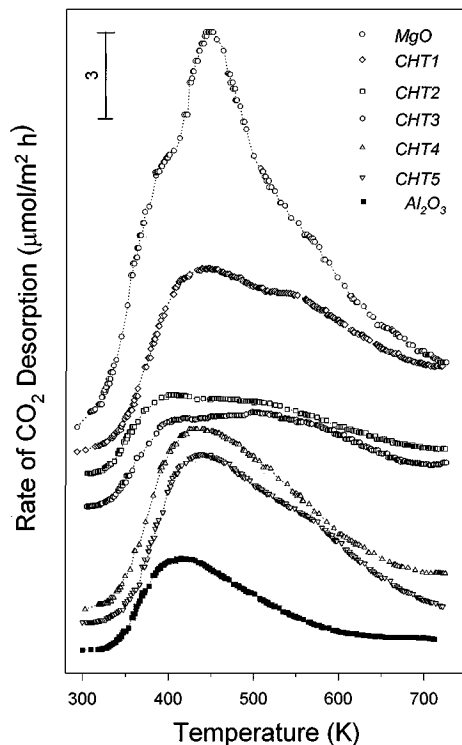

FIG. 5. TPD profiles of CO_2 on MgO, Al_2O_3, and CHT samples.

evolved CO_2 was obtained by integration of TPD curves. The resulting values are reported in the last column in Table 3 and show that the amount of evolved CO_2 on MgO is clearly higher than on CHT samples. The CO_2 TPD profiles on pure MgO and CHT samples are qualitatively similar and can be deconvoluted in three desorption bands, reaching maximum desorption rates at about 373, 443, and 543 K. We calculated by integration the relative contribution of each individual desorption peak. Results are presented in Table 3. The high-temperature peak is predominant on pure MgO, representing 59.3% of the total evolved CO_2, but the relative contribution of the low- and middle-temperature peaks increase with increasing the Al content in CHT samples. Thus, on sample CHT5 the high-temperature peak accounts for only 32.6% of the total desorbed CO_2.

Figure 6 shows the infrared spectra obtained on sample CHT4 after CO_2 adsorption at room temperature and sequential evacuation at 373, 473, and 573 K. Similar spectra were observed on all CHT samples. The spectra of MgO and Al_2O_3 samples are also included as reference. Three species of adsorbed CO_2, which are shown in Scheme 1, were detected (17, 18), apparently reflecting three different types of surface basic sites. Unidentate and bidentate carbonate formation requires surface basic oxygen atoms. Unidentate carbonates exhibit a symmetric O-C-O stretching at 1360–1400 cm^{-1} and an asymmetric O-C-O stretching at 1510–
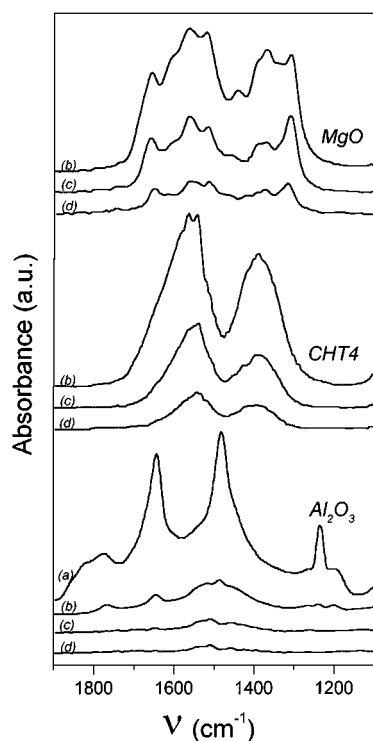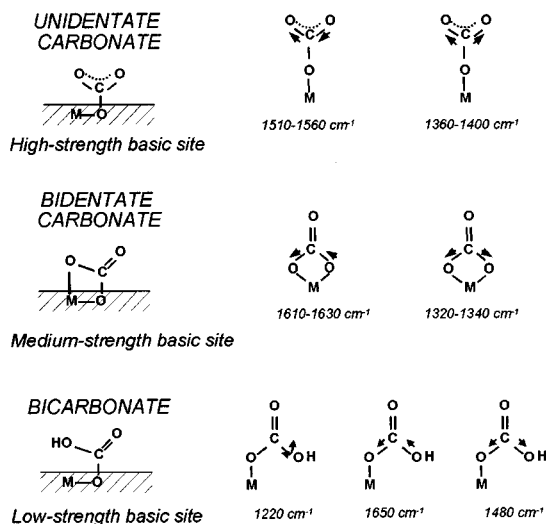

SCHEME 1. IR bands of adsorbed CO_2 surface species [after (17, 18)].

1560 cm^{-1}. Bidentate carbonates show a symmetric O-C-O stretching at 1320–1340 cm^{-1} and an asymmetric O-C-O stretching at 1610–1630 cm^{-1}. Bicarbonate species formation involves surface hydroxyl groups. Bicarbonates show a C-OH bending mode at 1220 cm^{-1} as well as symmetric and asymmetric O-C-O stretching modes at 1480 cm^{-1} and 1650 cm^{-1}, respectively.

Overlapping broad infrared bands were observed on pure MgO and CHT samples in the 1700–1500 cm^{-1} region following the CO_2 adsorption at room temperature. Similar qualitative spectra were obtained for all the samples after evacuation at each temperature, as is illustrated in Fig. 6 for pure MgO and sample CHT4. The bicarbonate species disappeared after evacuation at 373 K, but unidentate and bidentate carbonates remained on the surface even after evacuation at 573 K; after evacuation at 623 K, only unidentate carbonates species were detected. Figure 6 also shows that bicarbonate was clearly the predominant species formed on Al_2O_3 upon CO_2 adsorption at room temperature. After sequential evacuation at 373, 473, and 573 K, the bicarbonates were removed completely from the alumina surface.

Catalytic Conversion of Ethanol on Mg-Al Mixed Oxides

The rate and selectivity for ethanol conversion reactions were determined on CHT samples at 573 K. Ethanol is converted on Mg-Al calcined hydrotalcites via three main groups of reactions: dehydrogenation, coupling, and dehydration. In order to identify primary and secondary products, the effect of contact time on the product distribution was investigated using sample CHT4. It was found that dehydrogenation of ethanol forms acetaldehyde as a primary product. The consecutive aldol condensation of acetaldehyde yields n-butanol. Dehydration reactions lead to

FIG. 6. Infrared spectra of CO_2 adsorbed on MgO, Al_2O_3, and sample CHT4 upon increasing evacuation temperatures: (a) room temperature; (b) 373 K; (c) 473 K; (d) 573 K.
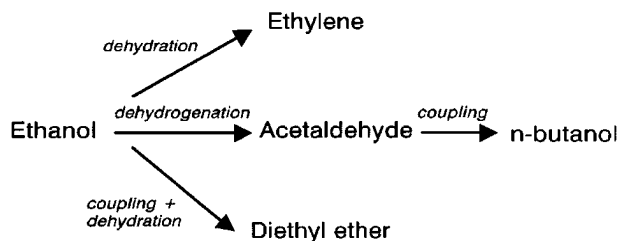
SCHEME 2. Reaction network of ethanol conversion.

diethyl ether and ethylene. A simplified reaction network of the ethanol conversion is shown in Scheme 2.

The catalytic results obtained on MgO, Al_2O_3, and CHT samples are shown in Table 4. Samples deactivated during the experiments and lost about 50% of activity after 10 h on stream. Rates in Table 4 are initial activities obtained by extrapolating conversion versus time curves to zero. Pure MgO shows very low reaction rates. On CHT samples, ethanol conversion rates depend on the Al content. Acetaldehyde formation is favored at low Al content while condensation to form *n*-butanol reaches a maximum rate on sample CHT4. The formation rate of ethylene and diethyl ether on CHT samples increase with the Al content. The alumina sample is especially active for producing ethylene. Table 4 shows that the ethylene formation rate on Al_2O_3 was almost two orders of magnitude higher than on sample CHT5, the most active CHT sample. Dehydration reactions appear to occur on Lewis or Brønsted acid sites present on Al_2O_3 surfaces that become abundant in Al-rich CHT samples.

DISCUSSION

Structure and Homogeneity of Hydrotalcite Precursors

The structure of precipitated samples is consistent with the predominant presence of rhombohedral hydrotalcite-

TABLE 4

Catalytic Results on MgO, Al_2O_3, and CHT Samples

Sample	Ethanol conversion rate (μmol/h m^2)	Formation rate (μmol/h m^2)			
		Acetaldehyde	*n*-Butanol	Diethyl ether	Ethylene
MgO	0.89	0.28	0.21	0.03	0.04
CHT1	8.35	4.64	0.96	0.26	0.06
CHT2	4.24	2.55	0.49	0.08	0.07
CHT3	4.55	1.10	1.00	0.19	0.08
CHT4	9.17	0.29	1.82	2.02	0.57
CHT5	9.84	0.26	0.52	3.89	0.60
Al_2O_3	48.15	0.08	0.00	4.84	28.57

Note. $T = 573$ K, $P = 100$ kPa, $W/F^0 = 46$ g h/mol, N_2/ethanol $= 10$ (molar).

like compounds consisting of positively charged brucite-like layers $[M_6^{II}M_2^{III}(OH)_{16}]^{2+}$ alternating with disordered negatively charged interlayers (19). The interlayer spacing is occupied by charge-compensating CO_3^{2-} anions and by weakly bonded water molecules. Several studies have discussed the successful synthesis of $Mg_{(1-x)}$-Al_x hydrotalcites with low Al content, but few reports have addressed the synthesis of HT samples with high Al content ($x > 0.50$). The synthesis conditions used in this work led to the formation of Mg-Al layered double hydroxides with uniform hydrotalcite structure and a broad range of Al content ($x = 0.10$–0.67).

The lattice parameter *a* of HT samples decreased monotonically, following Vegard's law dependence as the Al content increases (Fig. 1), suggesting that the brucite-like sheets can accommodate Al^{3+} cations within a wide compositional range. This contraction of the HT unit cell was previously reported for similar Mg-Al hydrotalcites (20–22). It appears to be caused by the formation of a solid solution, which is structurally stable in brucite layers because Al^{3+} cations replace larger Mg^{2+} cations in the brucite structure. Thus, Al^{3+} can randomly and uniformly replace Mg^{2+} in octahedral sites within brucite layers without disrupting the layer structure.

Influence of the Chemical Composition on the Structure of the Mixed Oxides

The thermal decomposition of $Mg_{(1-x)}Al_x$ hydrotalcites occurs in two steps (23). Below 453 K, weakly held water of hydration is desorbed. In the 453–673 K temperature range, water and CO_2 are formed by dehydroxylation of vicinal OH groups within brucite layers and by decarboxylation of interlayer CO_3^{2-}, respectively. The evolution of these gaseous products creates a significant porous structure and leads to the marked increase in surface area observed upon decomposition of HT samples. Al-rich hydrotalcite precipitates contain larger amounts of CO_2, because higher densities of CO_3^{2-} anions are required to compensate the net positive charge in the brucite layer. The resulting larger amounts of CO_2 evolved during decomposition cause the higher surface areas observed in Al-rich CHT samples (Table 2). Diffraction patterns of CHT samples showed no residual hydrotalcite or hydroxide phase, confirming that heating at 673 K leads to complete decomposition of HT samples. A poorly crystalline MgO phase was detected in all CHT samples, but no crystalline AlO_y phase was observed. The latter shows that Al^{3+} cations remain closely associated with the MgO structure after decomposition of HT samples within the entire compositional range of our study.

Several studies based on NMR analysis have proposed that Al coordination partially changes from octahedral to tetrahedral upon decomposition of hydrotalcites (11, 12, 23–25). Corma *et al.* (12) detected, in calcined hydrotalcites,

the presence of tetrahedrally coordinated Al^{3+} ions (Al_{Td}), which causes a ^{27}Al NMR band different from that of Al_{Td} located in a pure Al_2O_3 structure. Consequently, they proposed that part of the Al_{Td} ions are in tetrahedral sites within the MgO lattice. They found, however, that the amount of Al_{Td} increases with the Al content in the calcined hydrotalcite. The presence of Al_{Td} in the MgO structure leads to a decrease in the lattice constant of MgO (26). The diffraction patterns of our CHT samples, however, did not show any measurable lattice contraction with the Al content (Table 2), probably because of the poor crystallinity of hydrotalcite precursors decomposed at low temperatures (673 K). At high Al contents (sample CHT5, $x = 0.67$) a separate $MgAl_2O_4$ phase begins to form; its structure consists of a partially inverse spinel containing 44% of the Al^{3+} ions within tetrahedral positions (27). Thus, it is possible that some of the Al^{3+} cations are located in tetrahedral sites within MgO structures even for samples with lower Al content. This unstable structure may well generate small and distorted structures with partially inverse spinel ordering, which are difficult to detect by X-ray diffraction methods.

Surface Properties and Reactivity of the Basic Sites

Temperature-programmed desorption profiles of chemisorbed CO_2 suggest that several binding sites are available on the surface of MgO and of CHT samples. TPD profiles (Fig. 5) consist of three overlapping CO_2 desorption peaks, reaching maximum desorption rates at about 373, 443, and 543 K. The presence of three distinct adsorbed structures is also apparent from the infrared spectra of CO_2 adsorbed on CHT samples after partial desorption by evacuation at various temperatures (Fig. 6). In TPD experiments, the low-temperature desorption peak corresponds to bicarbonate species adsorbed on weakly basic OH groups; bicarbonate infrared bands disappear after treatment at 373 K. Bidentate carbonates adsorb on Mg-O site pairs and remain adsorbed until samples are treated above 573 K. Unidentate carbonates form on strongly basic surface O^{2-} anions and remain adsorbed even after evacuation at 623 K. Bidentate and unidentate carbonates have been assigned to CO_2 adsorbed on sites with intermediate and high basic strength, respectively (28).

$^{13}CO_2/^{12}CO_2$ isotopic exchange reactions follow first-order kinetics and relaxation curves follow straight lines in semi-logarithmic plots when adsorption–desorption processes occur on a single type of surface site. The slope in these plots reflects the rate constant for isotopic exchange. Large values of this rate constant reflect short $^{13}CO_2$ surface lifetimes corresponding to weaker binding of CO_2 on basic sites. The nonlinear behavior of the data in Fig. 3 confirms that the surface of MgO and CHT samples is nonuniform and that it contains sites with varying exchange kinetics and basic strength. The data in Fig. 3 can be described by first-order exchange processes occurring on two types of

sites with widely different desorption rate constants. As expected, isotopic exchange methods cannot detect weakly adsorbed bicarbonate species, because OH surface sites are largely uncovered at the temperatures of the exchange experiments and of catalytic interest. Bidentate species account for the rapid exchange processes at short times and more strongly adsorbed unidentate species for the exchange process occurring at longer times.

Compositional Effects on Basic Site Density and Strength

The $^{13}CO_2/^{12}CO_2$ isotopic exchange data in Fig. 4 show that basic site densities (per unit surface area) on CHT samples depend on Al content. The density of basic sites on pure MgO decreases when small amounts of Al are added. Basic site densities on CHT samples with x values between 0.1 and 0.2 are less than half of the corresponding values measured on pure MgO. The density of basic sites then increases as additional Al is added, reaches a maximum for CHT samples with x values of about 0.5, but never recovers the site density values characteristic of pure MgO. Qualitatively similar trends were obtained when site densities are calculated from the area under CO_2 temperature-programmed desorption profiles (Table 3), which include both strongly held and weakly held CO_2.

The effect of the Al content on the basicity of calcined Mg-Al hydrotalcites was studied by Fishel et al. (25) (for $x = 0.17–0.33$) and by Nakatsuka et al. (29) ($x = 0.10–0.44$). Nakatsuka et al. (29) reported that the basic site density measured by titration with benzoic acid (strength $H_- \geq 15$) depends on the Al content, reaching a maximum for x values of about 0.28. Fishel et al. (25) measured the number of basic sites by TPD of CO_2 and observed that the basic site density of pure MgO decreases when small amounts of Al are added; then it increases for higher x values, reaching a maximum at ca $x = 0.25$. Derouane et al. (24) studied the physicochemical properties of Mg-Al calcined hydrotalcites with $x = 0.17–0.33$ and found that both the crystallinity and the unit cell of pure MgO decrease with the Al content. These results were attributed to the migration of Al^{3+} ions into the MgO framework, which creates a cationic vacancy; the surface then acts as a sink for the vacancy and one Mg^{2+} is removed from the surface leading to the formation of an additional surface O^{2-} ion. They postulated that oxygen-terminated, negatively charged (111) planes in MgO would be then more suitable than magnesium-oxygen-terminated (100) planes to accommodate additional oxygen atoms.

Using Derouane's model, Fishel et al. (25) explained the CO_2 chemisorption capacity decrease observed on ex-hydrotalcites of low Al content by postulating that the oxygen-terminated (111) planes would be less likely to chemisorb CO_2. They assumed the need of exposed Mg^{2+}-O^{2-} pairs, which are not favored on (111) planes, in order for the chemisorption of CO_2 to take place. However, our TPD and IR results show that at low x values,

the CO_2 chemisorption takes place not only on medium-strength Mg^{2+}-O^{2-} pairs, but also on strongly basic surface O^{2-} ions. About 45% of the chemisorbed CO_2 gave rise to unidentate carbonates formed on high-strength O^{2-} ions (Table 3). Furthermore, X-ray photoelectron results show that Mg_s/O_s ratios on CHT samples with low Al content (1.16–1.26) were similar to that on pure MgO (1.20) (Table 3). The nearly equimolar amounts of Mg and O on the surface of these samples suggest the presence of abundant exposed Mg^{2+}-O^{2-} pairs and excludes a preferential (111) surface orientation.

Our X-ray photoelectron results show significant Al surface enrichment in CHT samples with low Al content ($Al_s/Al_b = 2.30$–2.68, Table 3), suggesting a more plausible explanation for the decrease in basic site density observed on these samples. The Al^{3+} migration to the surface in samples with low Al content was predicted by Rohrer *et al.* (30) using Monte Carlo simulations of Mg(Al)O solid solutions. These simulations showed that for a sample with $x = 0.17$ the effects of Schottky defects and Al^{3+} ions on the atomic relaxations at the MgO surface cause substitutional Al^{3+} ions and cation vacancies to segregate to the surface region, in accordance with experimental observations. The presence of more electronegative amorphous AlO_y structures or isolated Al centers on MgO surfaces blocks CO_2 chemisorption sites, which are five times more abundant on pure MgO than on pure Al_2O_3 (Table 3, last column). At higher Al contents, the Al_s/Al_b ratio decreases, suggesting that surface segregation of Al is less likely to occur, and basic site densities then increase (Fig. 4) concurrently with increases in surface oxygen concentrations (Fig. 2). While no separation of phases takes place, the Al^{3+} cations located in the MgO framework create a defect in order to compensate the positive charge generated, and the adjacent oxygen anions become coordinatively unsaturated; as a result, the solid solution displays higher basicity. As the bulk spinel is formed, the Al^{3+} cations leave the MgO lattice and phase segregation occurs causing the density of basic sites to drop.

The increase in Al content influences both the basic site density, as measured by $^{13}CO_2/^{12}CO_2$ isotopic exchange, and the surface oxygen concentration (Figs. 4 and 2), which strongly suggests that surface oxygen (as O^{2-} anions and in Mg^{2+}-O^{2-} pairs) provides the binding sites for adsorbing CO_2 at the temperatures of the exchange measurements. The effect of Al content on the distribution of basic site strength in CHT samples was investigated by decomposing the CO_2 TPD curves of Fig. 5 into three desorption peaks and measuring their respective areas. Results presented in Table 3 show that pure MgO exhibits the highest relative concentration of high-strength basic sites. Consequently, the relative contribution of low- and medium-strength basic sites on CHT samples is higher than on MgO. This is consistent with the observed shift in the binding energy of the O 1s XPS line from its value for O^{2-} species on pure MgO

to values corresponding to OH^- groups as the Al content increases (Table 3). Also, the infrared spectra of adsorbed CO_2 in Fig. 6 show that only weakly bonded bicarbonate species on basic OH^- groups are formed on pure Al_2O_3. Therefore, we conclude that the formation of weakly basic OH groups on CHT samples increases with the Al content and, as a result, the average surface basic strength diminishes.

Compositional Effects on Catalytic Activity

The product distribution in ethanol conversion reactions is influenced by the surface acid–base properties. We have shown that the CHT $Mg_{1-x}Al_xO$ samples present three different types of basic sites: isolated O^{2-} ions, Mg^{2+}-O^{2-} pairs, and OH groups; their relative concentrations depend on the Al content. Also, we found that the contribution of Al^{3+}-O^{2-} pairs to the surface basicity is not important. In contrast, the surface Lewis acidic sites are provided by both Mg^{2+} and Al^{3+} cations. The Lewis acidity supplied by the metal cations is stronger than that of the Brønsted OH groups (38).

Table 4 shows that acetaldehyde was the predominant product on CHT samples with low Al content. Dehydrogenation of a primary alcohol to the corresponding aldehyde is usually faster than alcohol dehydration on basic oxides and this reaction appears to require large polarizable cations, such as the alkaline earths ions (32–34). Dehydrogenation involves the initial adsorption of ethanol on an acid–strong base pair site, which breaks the O-H bond forming a surface ethoxy intermediate. Then, the α-hydrogen in the ethoxy group is abstracted by another strong basic site. The acetaldehyde formation mechanism is represented in Scheme 3, where A and B are Lewis acid sites and Brønsted basic sites, respectively:
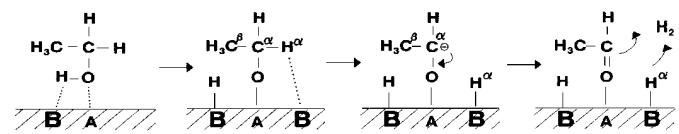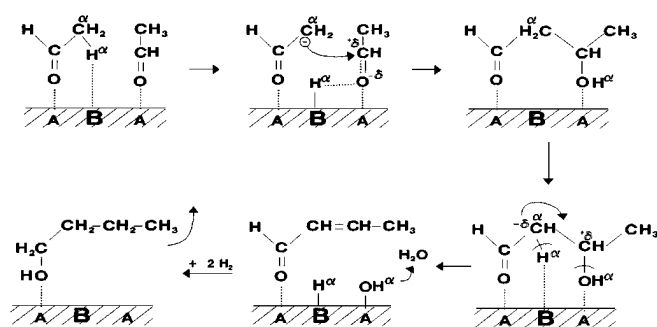

SCHEME 3

Pure MgO catalyzes the dehydrogenation of ethanol to acetaldehyde at very low rates. This is consistent with the predominant presence of isolated surface O^{2-} ions on MgO surfaces. Isolated O^{2-} basic centers would be unable to form ethoxide intermediates, which requires acid–strong base pair sites. The rate of formation of acetaldehyde on CHT samples with low Al content ($x < 0.2$) was about one order of magnitude higher than on pure MgO. It appears that the addition of small amounts of Al drastically increases the surface density of active acid–strong base pair sites. Our XPS and CO_2 TPD results showed significant Al surface enrichment in CHT samples with low Al content, which

counterbalanced the contribution of high-strength basic sites. The enhanced acetaldehyde production observed on samples CHT1 and CHT2 may be interpreted then by assuming that these samples contain a much larger number of properly positioned Al^{3+} Lewis acid sites and Mg^{2+}-O^{2-} basic pairs, which catalyze the rate-limiting step in the ethanol dehydrogenation mechanism.

Condensation of adsorbed acetaldehyde species is faster than dehydrogenation (32), so that formation of coupling products on basic oxides is expected to be rather important. However, whereas the acetaldehyde formation on CHT samples decreases monotonically with Al content, its consecutive coupling to n-butanol reaches a maximum for sample CHT4. Similarly to ethanol dehydrogenation, the aldol condensation of acetaldehyde to n-butanol on basic oxides involves formation of a carbanion intermediate on an acid-strong base pair site:
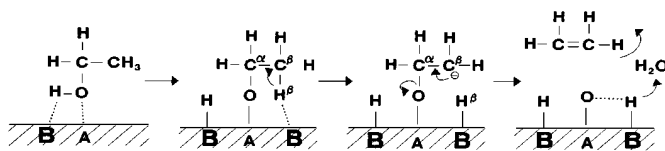

SCHEME 4

Acetaldehyde condensation, however, is a bimolecular reaction between adjacent adsorbed acetaldehyde species, and the formation of n-butanol requires not only acid-strong base pair sites but also a high density of basic sites. We found that sample CHT4 contains the highest density of basic sites among the CHT samples (Fig. 4) and this may explain the high rate of n-butanol synthesis on this sample. For similar reasons, the aldol condensation to n-butanol is unlikely to take place on pure Al_2O_3 surface.

In addition to n-butanol, at least two other products are predicted to form from acetaldehyde condensation. The partially hydrogenated intermediate compound, n-butyraldehyde, was detected on CHT samples of high Mg contents in concentrations that represent less than 3% of the overall reaction rate. On the other hand, the α,β-unsaturated aldol-type species (2-butenal) depicted in Scheme 4, which is expected to interact strongly with the basic surface, was never observed. It appears that the migration and recombination of surface hydrogen atoms resulting from formation of adsorbed acetaldehydic species take place faster than the α,β-unsaturated intermediate desorption, thereby favoring the complete hydrogenation of 2-butenal to n-butanol.

Dehydration of alcohols occurs on oxides containing small-highly charged cations (32) which exhibit acidic properties. Olefin formation is the predominant reaction on acidic oxides, but ether formation can also take place (35–37). Ethanol dehydration to ethylene on Mg-Al mixed oxides proceeds via two mechanisms. The E_{1cB} mechanism requires both strongly basic sites and weak Lewis acid sites (34, 38). Initially, the adsorption of the ethanol molecule and the O-H bond rupture on the acid–strong base pair site gives rise to a surface ethoxy group. Then, the E_{1cB} mechanism leads to the abstraction of the most acidic proton in the ethoxy intermediate on the basic site, with formation of a carbanion by C^β-H^β bond rupture (39). Formation of the olefin takes place in the final step:

SCHEME 5

The E_2 elimination is a concerted single-step mechanism which involves Lewis acidic and basic sites of balanced strength so that no formation of ionic intermediate takes place. The acidic site responsible for the OH abstraction, should be stronger than the one participating in the E_{1cB} mechanism:
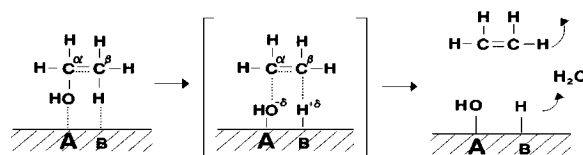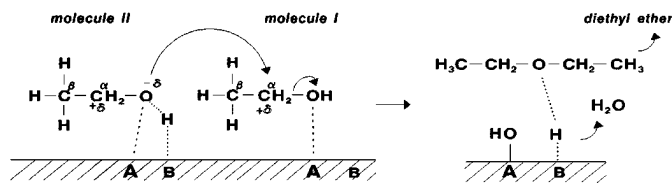

SCHEME 6

Table 4 shows that ethylene is readily formed on alumina, which is a typical E_2 catalyst (33). Alumina was two or three orders of magnitude more active for ethylene production than CHT samples. On CHT samples, ethylene formation rates increased with increasing Al content. Samples CHT5 and CHT4 contain a relatively high density of Al^{3+}-O^{2-} pairs and a lower density of strong basic sites (Table 3). Ethylene formation on these samples would occur then through an E_2 mechanism. In contrast, on CHT samples with low Al content, the density of strong basic sites is much higher than that of the acid sites generated by the aluminum surface enrichment and the ethylene formation rates decrease. On Mg-rich samples (samples CHT1 and CHT2), dehydration of ethanol to ethylene probably occurs via an E_{1cB} mechanism, which requires strong basic sites. The olefin formation on pure MgO has already been ascribed to an E_{1cB} mechanism (38).

Formation of diethyl ether from ethanol on alumina is a second-order reaction that involves two adjacent alcohol

molecules adsorbed on two different types of site (35, 40). One alcohol molecule (I) adsorbs on a Lewis acid site through the oxygen of the OH group, and the C^α atom becomes slightly positive. The other ethanol molecule (II) adsorbs on a basic site via a H-bond that increases the nucleophilicity of the oxygen in the OH group. The adsorbed molecule II is an incipient alkoxide ion (35) which then performs a nucleophilic displacement on the C^α atom of the molecule I to form diethyl ether:

SCHEME 7

It has been debated in the literature whether formation of olefin and ether from primary alcohols takes place on acid sites of similar or different acid strengths. Ross *et al.* (41) studied the effect of Na^+ doping on the dehydration of ethanol over alumina. They showed that the increase in the Na content leads to a shift in the selectivity from ethylene to diethyl ether. Consistently, Jain *et al.* (35) reported that the alcohol dehydration to olefins has a higher activation energy than the competitive dehydration to ethers and will be favored then by the presence of stronger surface acidic sites or the use of higher reaction temperatures.

Table 4 shows that the formation rates of both diethyl ether and ethylene increase with increasing Al content in calcined hydrotalcites. However, results of Table 4 suggest different acid–base site requirements for ethylene and diethyl ether formation. Low selectivities to ethylene were found in the entire compositional range of calcined hydrotalcites; diethyl ether was one of the main products only on CHT samples of high Al/(Al + Mg) ratios. This suggests that at high Al contents, the combination of surface properties, as discussed above, generates acid–base pair sites acidic enough to catalyze the synthesis of diethyl ether rather than the olefin formation through an E_2 mechanism. It has to be noted here that several authors have found that the adsorption of alcohols over basic oxides takes place also on weaker Brønsted acidic sites provided by surface OH groups (31, 34). Noller *et al.* (31) reported that the ethanol adsorption mode shown for the ethanol molecule I in Scheme 7, takes place on surface hydroxyl groups rather than on Lewis sites such as Mg^{2+} or Al^{3+} ions. From our results, the participation of surface OH groups in the synthesis of diethyl ether cannot be ruled out because diethyl ether formation rates on CHT samples parallel the extent of surface hydroxylation determined by XPS (Table 3).

CONCLUSIONS

The nature, density, and strength of surface basic sites on ex-hydrotalcite Mg-Al mixed oxides depend on the sample composition. In samples of low Al content ($x < 0.2$), the basic site density is clearly lower as compared to pure MgO because the formation of a surface AlO_y phase partially covers the Mg-O pairs and decreases the concentration of surface O^{2-} anions. At higher Al contents ($0.2 < x < 0.5$), a highly interacting Mg-Al oxide phase is formed by incorporation of Al^{3+} ions into the MgO matrix and causes the number of surface defects to increase and the partial recovery of the basic site density. In samples with $x > 0.5$, demixing of the Mg-Al phase occurs leading to bulk $MgAl_2O_4$ spinels. As a result, the basic site density diminishes.

On pure MgO, strong basic sites consist predominantly of O^{2-} anions. Calcined hydrotalcites contain surface sites of low (OH^- groups), medium (Mg-O pairs), and strong (O^{2-} anions) basicity. Their relative abundance depends on the chemical composition; the surface concentration of low and medium strength basic sites increases with increasing Al content in the sample.

The catalyst activity and selectivity of CHT samples in ethanol reactions also depend on composition. Reactions requiring strong basic sites, such as dehydrogenation, condensation, and E_{1cB} dehydration, involve the initial surface ethoxide formation on a Lewis acid–strong base pair site. Pure MgO exhibits poor activity because the predominant presence of isolated O^{2-} basic centers hinders ethanol dissociative adsorption steps that form the ethoxide intermediate. MgO forms predominantly acetaldehyde and *n*-butanol via reactions favored on strongly basic materials.

The incorporation of small amounts of Al to MgO increases ethanol reaction rates by about one order of magnitude. It appears that Al^{3+} cations drastically increase the surface density of active Lewis acid–strong base pair sites. Calcined Mg-Al hydrotalcites with low Al content selectively dehydrogenate ethanol to acetaldehyde. The consecutive coupling of acetaldehyde to *n*-butanol demands, in addition to the Lewis acid–strong base center, a higher density of basic sites; therefore these pathways are favored on CHT samples with higher Al content ($0.2 < x < 0.5$).

Ethanol dehydration rates increase abruptly on samples containing a high density of both Al^{3+}-O^{2-} pairs and low- and medium-strength basic sites. Thus, the formation of ethylene and diethyl ether from ethanol occurs mainly on CHT samples with high Al content. Pure alumina displays the highest total activity, however, dehydrogenation and condensation products do not form because of the absence of acid–strong base pair sites.

REFERENCES

1. Constantino, V. R. L., and Pinnavaia, T. J., *Inorg. Chem.* **34**(4), 883 (1995).
2. Cavani, F., Triffiro, F., and Vaccari, A., *Catal. Today* **11**, 173 (1991).
3. Sugier, A., and Freund, E., U.S. Patent 4,112,110, Institut Français du Pétrole, 1978.
4. Alcaraz, J. J., Arena, B. J., Gillispie, R., and Holmgren, J. S., *in* "Proceedings, 15th Meeting of the North American Catalysis Society, Chicago, 1997." p. 114.
5. Ginés, M. J. L., Amadeo, N., Laborde, M., and Apesteguía, C. R., *Appl. Catal.* **131**, 283 (1995).
6. Di Cosimo, J. I., Díez, V. K., Apesteguía, C. R., Xu, M., and Iglesia, E., *in* "Proceedings, 15th Meeting of the North American Catalysis Society, Chicago, 1997." p. 58.
7. Reiche, W. T., *J. Catal.* **94**, 547 (1985).
8. Velu, S., and Swamy, C. S., *Appl. Catal.* **119**, 241 (1994).
9. Corma, A., Iborra, S., Primo, J., and Rey, F., *Appl. Catal.* **114**, 215 (1994).
10. Ginés, M. J. L., Iglesia, E., Di Cosimo, J. I., and Apesteguía, C. R., in preparation.
11. Schaper, H., Berg-Slot, J. J., and Stork, W. H. J., *Appl. Catal.* **54**, 79 (1989).
12. Corma, A., Fornés, V., and Rey, F., *J. Catal.* **148**, 205 (1994).
13. Xu, M., Ginés, M. J. L., Hilmen, A., Stephens, B. L., and Iglesia, E., *J. Catal.* **171**, 130 (1997).
14. Padró, C. L., Grosso, W. E., Baronetti, G. T., Castro, A. A., and Scelza, O. A., *in* "New Developments in Selective Oxidation" (V. Cortés Corberán and S. Vic Bellón, Eds.), p. 411. Elsevier, Amsterdam, 1994.
15. Peng, X. D., Richards, D. A., and Stair, P. C., *J. Catal.* **121**, 99 (1990).
16. Balakrishnan, K., and Schwank, J., *J. Catal.* **127**, 287 (1991).
17. Morterra, C., Ghiotti, G., Boccuzzi, F., and Coluccia, S., *J. Catal.* **51**, 299 (1978).
18. Philipp, R., and Fujimoto, K., *J. Phys. Chem.* **96**, 9035 (1992).
19. Taylor, H. F. W., *Min. Mag.* **39**(304), 377 (1973).
20. Pausch, I., Lohse, H. H., Schurmannand, K., and Allmann, R., *Clays Clay Min.* **34**, 507 (1986).
21. Miyata, S., *Clays Clay Min.* **28**, 50 (1980).
22. Kooli, F., Kosuge, K., and Tsunashima, A., *J. Mater. Sci.* **30**, 4591 (1995).
23. Reichle, W. T., Kang, S. Y., and Everahardt, D. S., *J. Catal.* **101**, 352 (1986).
24. Derouane, E. G., Jullien-Lardo, V., Davis, R. J., Blom, N., and Hojlund-Nielsen, P. E., *in* "New Frontiers in Catalysis" (L. Guczi, L. Solymosi and P. Tetenyi, Eds.), Vol. B, p. 1033. Elsevier, Amsterdam, 1993.
25. Fishel, C. T., and Davis, R., *Langmuir* **10**(1), 159 (1994).
26. Sato, T., Fujita, H., Endo, T., and Shimada, M., *Reactivity of Solids* **5**, 219 (1988).
27. Mc Clure, D., *J. Phys. Chem. Solids* **3**, 311 (1957).
28. Kanno, T., and Kobayashi, M., *in* "Acid-Base Catalysts II" (M. Misono and Y. Ono, Eds.), p. 207. Kodansha-Elsevier, Tokyo, 1994.
29. Nakatsuka, T., Kawasaki, H., Yamashita, S., and Kohjiya, S., *Bull. Chem. Soc. Japan* **52**, 2449 (1979).
30. Rohrer, C. L., and Rohrer, G. S., *Chem. Mater.* **6**, 501 (1994).
31. Noller, H., and Ritter, G., *J. Chem. Soc. Faraday Trans.* **1**(80), 275 (1984).
32. Kibby, C. L., and Hall, W. K., *J. Catal.* **29**, 144 (1973).
33. Tanabe, K., Misono, M., Ono, Y., and Hattori, H., "New Solid Acids and Bases," Kodansha-Elsevier, Tokyo, 1989.
34. Canesson, P., and Blanchard, M., *J. Catal.* **42**, 205 (1979).
35. Jain, J. R., and Pillai, C. N., *J. Catal.* **9**, 322 (1967).
36. Padmanabhan, V. R., and Eastburn, F. J., *J. Catal.* **24**, 88 (1972).
37. Luy, J. C., and Parera, J. M., *Appl. Catal.* **26**, 295 (1986).
38. Gervasini, A., Fenyvesi, J., and Aroux, A., *Catal. Lett.* **43**, 219 (1997).
39. Winterbottom, J. M., *in* "Catalysis," Vol. 4, p. 141. The Royal Society of Chemistry, Burlington House, London, 1981.
40. Balaceanu, J. C., and Jungers, J. C., *Bull. Soc. Chim. Belg.* **60**, 476 (1951).
41. Ross, R. A., and Bennett, D. E. R., *J. Catal.* **7**, 289 (1967).